siRNA in human cells selectively localizes to target RNA sites

Svitlana Y. Berezhna*†, Lubica Supekova†‡, Frantisek Supek§, Peter G. Schultz‡¶, and Ashok A. Deniz*¶

Departments of *Molecular Biology (MB 19) and ‡Chemistry, The Scripps Research Institute, 10550 North Torrey Pines Road, La Jolla, CA 92037; and §Genomics Institute of the Novartis Research Foundation, 10675 John Jay Hopkins Drive, San Diego, CA 92121

Contributed by Peter G. Schultz, March 28, 2006

Recent observations of RNA interference (RNAi) in the nuclei of human cells raise key questions about the extent to which nuclear and cytoplasmic RNAi pathways are shared. By directly visualizing the localization of small interfering RNA (siRNA) in live human cells, we show here that siRNA either selectively localizes in the cytoplasm or translocates into the nucleus, depending on where the silencing target RNA resides. Two siRNAs that target the small nuclear 7SK and U6 RNAs localize into the nucleus as duplexes. In contrast, an siRNA targeting the cytoplasmic hepatitis C virus replicon RNA dissociates, and only antisense strand distributes in the cytoplasm of the cells harboring the target RNA, whereas sense strand gets degraded. At the same time, both strands of the latter siRNA are distributed throughout the cytoplasm and nucleus in cells lacking the silencing target RNA. These results suggest the existence of a mechanism by which the RNAi machinery orchestrates a target-determined localization of the siRNA and the corresponding RNAi activity, and also provide evidence for formation of nuclear-programmed active RNA induced silencing complexes directly in the nucleus.

confocal imaging | nuclear/cytoplasmic localization | RNA-induced silencing complex | RNA interference mechanism | small interfering RNA

Nearly a decade after the discovery that double-stranded RNA can trigger an RNAi response that inhibits gene expression in a sequence-specific manner (1), the complexity of the mechanisms by which small RNAs regulate gene expression continues to unfold (2–11). RNA interference (RNAi) has generally been defined as a cellular pathway that mediates posttranscriptional gene silencing either by sequence-specific degradation of targeted RNAs or via sequence-specific inhibition of translation. Thus, RNAi studies in mammalian cells have mainly focused on the cytoplasm, where mature mRNA is translated and key proteins of RNA-induced silencing complexes (RISCs) were thought to localize and function. These RISCs, by which the RNAi machinery implements silencing of gene expression, are composed of several proteins (including Ago1 and Ago2) and one strand of small interfering RNA (siRNA) (12, 13). During the course of RISC assembly, the siRNA/microRNA duplex dissociates, and the guide strand enters active RISCs, allowing binding and degradation of the complementary target mRNA.

Target specificity in RNAi is achieved through RNA–RNA sequence recognition and base pairing. Because RNA can also recognize and form duplexes with DNA, RNAi should be capable of affecting gene function at the level of genomic DNA, extending the realm of RNAi function into the nucleus. Indeed, recent demonstrations of siRNA-induced transcriptional gene silencing through involvement of DNA methylation (2, 3) in various human cell types, siRNA-dependent knock-down of nucleus-restricted transcripts (4, 5), and a direct documentation of potent and specific down-regulation of 7SK and U6 small nuclear RNAs (6) have uncovered such nuclear RNAi pathways in human cells. In the latter work, immunoblot analysis and activity assays confirmed the presence of the key RISC proteins Ago1 and Ago2, as well as functional RISC complexes, in both the cytoplasm and nuclei of HeLa cells. Given these results, different mechanisms can be envisioned by which nuclear-programmed RISCs are formed and localize to the nucleus. One possibility is that the guide (antisense) siRNA strand forms RISC in the cytoplasm, and this assembled and active RISC is then transported to the nucleus. This mechanism could represent a common RISC formation pathway for both cytoplasmic and nuclear targets, with subsequent cytoplasmic and nuclear partitioning of variously programmed RISC complexes. Alternately, siRNA could first enter the nucleus as duplexes, followed by active RISC assembly in the nucleus. A third possibility is that RISC complexes can be formed both in the cytoplasm and in the nucleus, with or without later redistribution in the cell. In a more general context, it is not known whether, after transfection, siRNA is randomly distributed and can form RISC complexes throughout the cell, or a more selective cytoplasmic versus nuclear distribution and localized activity is achieved through passive or active transport.

Results and Discussion

To investigate these mechanistic possibilities, we used confocal imaging to directly visualize the localization of fluorescently labeled siRNA after transfection in human Huh-7 hepatoma cells harboring the subgenomic hepatitis C virus (HCV) replicon. HCV replication occurs at the virus-induced specialized membrane structures derived from the endoplasmic reticulum, which are dispersed in the cytoplasm (14). In the imaging experiments, we separately examined the intracellular locations of two siRNA duplexes, 7SK siRNA targeting the small nuclear 7SK RNA (6, 15–17) and NS3 siRNA that targets the cytoplasmic HCV replicon RNA (18). Each siRNA duplex was labeled with Alexa Fluor 488 and Cy5 fluorophores at the 3′ ends of sense and antisense strands, respectively, to visualize the localizations of the two strands in the cells. All siRNAs were determined to be active, and labeled and unlabeled siRNAs had identical activities within error (Figs. 6 and 7, which are published as supporting information on the PNAS web site).

Two hours after transfection, both sense and antisense strands of 7SK siRNA clearly accumulate in the nuclei of Huh-7 HCV cells (Fig. 1). Antisense and sense siRNA strands were visualized by using their fluorescent labels, depicted in red (Fig. 1*a*) and green (Fig. 1*b*), respectively, and the nuclei of the cells were stained with DAPI (blue, Fig. 1*c*). In sharp contrast to these observations, Huh-7 cells identically transfected with NS3 siRNA exhibited a completely different localization behavior (Fig. 2). In the latter case, no visible accumulation of NS3 siRNAs was seen in the nucleus. Furthermore, significant strand-separation of NS3 siRNA was observed. The antisense NS3

Conflict of interest statement: No conflicts declared.

Abbreviations: RISC, RNA-induced silencing complex; RNAi, RNA interference; HCV, hepatitis C virus; siRNA, small interfering RNA.

†S.Y.B. and L.S. contributed equally to the work.

¶To whom correspondence may be addressed. E-mail: deniz@scripps.edu or schultz@scripps.edu.

www.pnas.org/cgi/doi/10.1073/pnas.0600148103

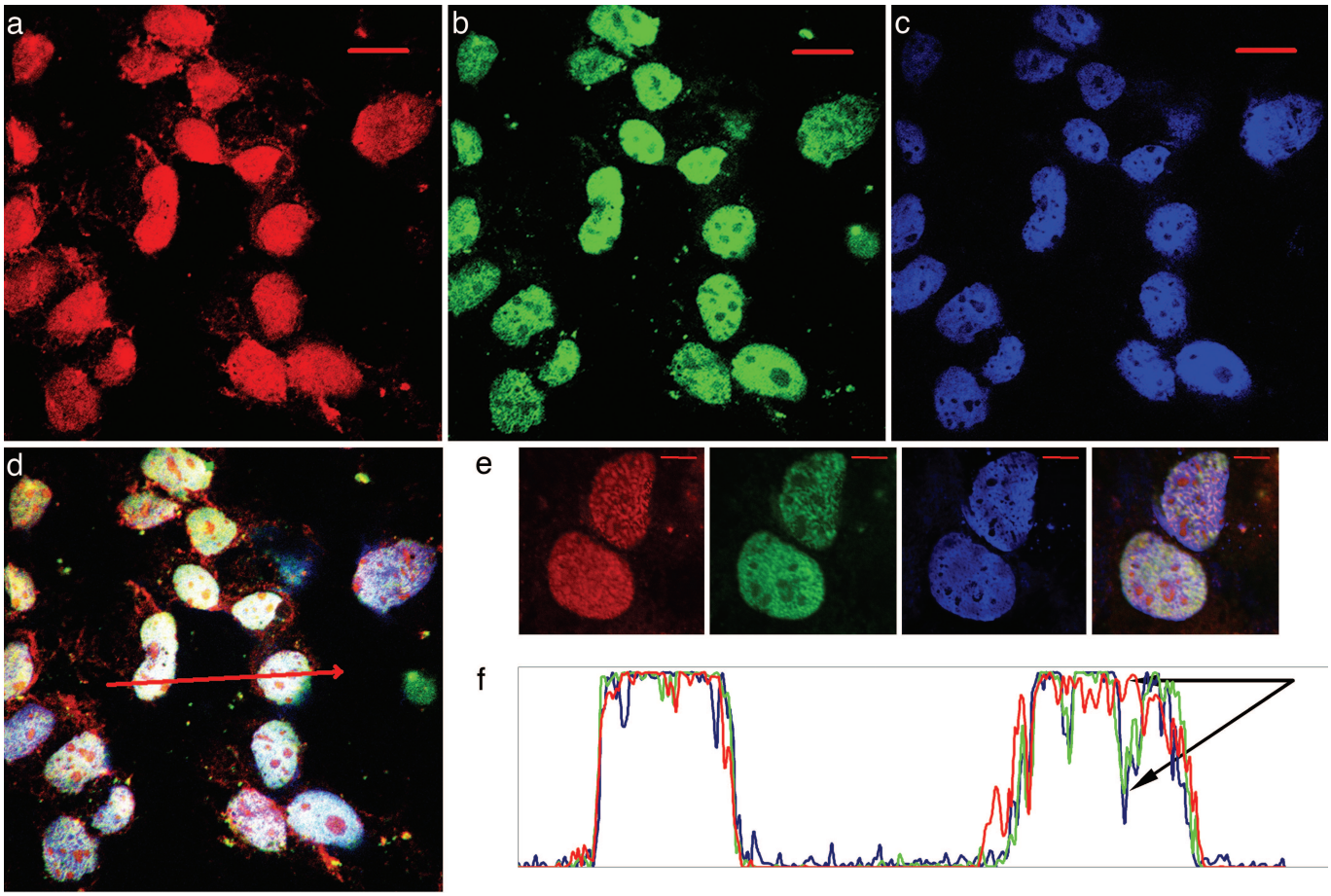

Fig. 1. 7SK siRNA accumulates in the nucleus in Huh-7 cells 2 h after transfection. (*a–c*) 7SK siRNA antisense (red) and sense (green) strands colocalize primarily in the nucleus (blue), seen in the cytoplasm only in small amounts. (Scale bar, 20 μm.) (*d*) Overlay of red, green, and blue. (e) Two cells. (Scale bar, 10 μm.) (*f*) Intensity profiles along the selected line (red arrow in *d*) across cells show that both siRNA strands enter the nucleus, where they apparently get separated, because primarily the antisense strand is visible in the nucleoli (marked by arrows, DAPI-depleted dark spots against a blue background in *c*).

siRNA strand was observed to create perinuclear ring-like patterns of clustered dots (seen in red in Fig. 2*d* around nuclei in blue), whereas the sense strand nearly disappeared and was only sparsely visible as distinct dots (Fig. 2*b*).

Colocalization of the three signal profiles (DAPI, Alexa Fluor 488, and Cy5) along multiple lines through the cells (examples are given in Figs. 1*f* and 2*f*) provided additional information about the distributions of these siRNAs. In the case of 7SK siRNA, a minor amount of the RNA could be found as a diffuse background in the cytoplasm but clusters were typically not observed to concentrate in the perinuclear area. Within the nuclear boundaries, the two strands showed different levels of accumulation in the nucleoli (Fig. 1*f*, arrows), which could signify partial strand separation. In the case of NS3 siRNA, sharp peaks of the red signal at the edges of nuclear boundaries verify that the two strands are separated, and the antisense strand tends to accumulate in the perinuclear area in distinct loci. Also, a very low level of NS3 siRNA sense strand was seen in the nucleus as a diffusely distributed pattern (Fig. 2*f*, the green line inside the nuclear boundaries marked by a wide blue plateau). In these experiments, no localization of the antisense NS3 siRNA strand to the nucleus was observed within the sensitivity of the detectors, using the highest available laser powers for excitation of the dyes. These contrasting 7SK siRNA and NS3 siRNA behaviors did not vary significantly at various times after transfection. In particular, the nuclear-targeted 7SK siRNA was clearly observed to accumulate in the nucleus as quickly as 40 min after transfection, whereas cytoplasmically targeted NS3 siRNA remains distributed largely in the cytoplasm 4 h after transfection, showing no nuclear accumulation. In addition, we also carried out 7SK siRNA transfection for HeLa cells, and observed similar behavior.

RISC assembly involves incorporation of the antisense siRNA strand into the complex, and therefore requires duplex siRNA strand separation (12, 13). Recent experiments have shown that Ago2 protein likely cleaves the sense strand after siRNA binding, resulting in the sense strand dissociation and only antisense strand incorporation into active RISC (10, 11). Therefore, RISC formation will be correlated with siRNA duplex strand separation in our imaging experiments. Furthermore, because the incorporated siRNA single strand is known to be tightly bound to Ago proteins in RISC (19), the localization of RISC is expected to parallel the observed siRNA antisense strand localization. Based on this premise, the observed patterns of Alexa Fluor 488 and Cy5 fluorescence in the NS3 siRNA images (Fig. 2) clearly demonstrate that strand separation and RISC formation occur in the cytoplasm. In addition, the nearly complete exclusion of sense strand from the cytoplasm and low levels of only this strand in the nucleus are also consistent with the idea of siRNA duplex dissociation and sense strand cleavage during NS3 siRNA RISC formation all occurring in the cytoplasm. Therefore, we would expect that, if active RISC formation for 7SK siRNA were also taking place in the cytoplasm followed by transport of this active RISC into the nucleus, the images in Fig.

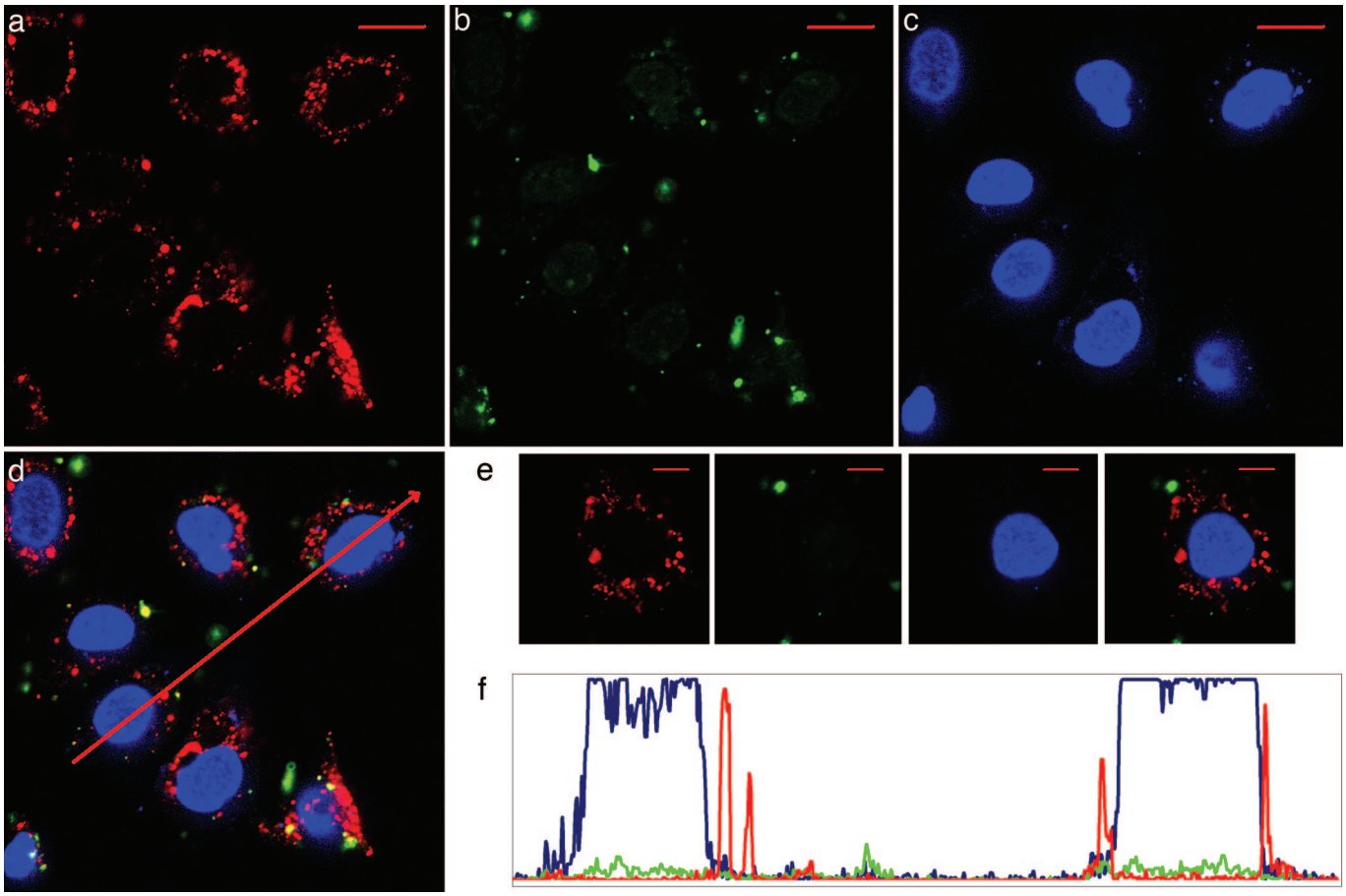

Fig. 2. NS3 siRNA appears restricted to the cytoplasm of Huh-7 cells 2 h after transfection. (*a–c*) NS3 siRNA antisense strand (red) is seen clustered in the perinuclear area but does not enter the nucleus (blue), whereas sense strand (green) is barely visible. (Scale bar, 20 μm.) (*d*) Overlay of red, green, and blue. (*e*) A single cell. (Scale bar, 10 μm.) (*f*) Intensity profiles along the selected line (red arrow in *d*) across cells confirm perinuclear antisense strand (red) localization and show that a small amount of sense (green) strand can be found within the nucleus (blue).

1 would show similar strand separation in the cytoplasm and sense strand distribution in the cell. Instead, we observe predominantly nuclear localization of both 7SK siRNA strands, leading us to conclude that this siRNA locates as a duplex to the nucleus in an efficient manner, without prior strand separation. Strand separation and formation of active RISC must then occur within the nucleus, resulting in the observed 7SK downregulation (see Fig. 6).

The 7SK and NS3 siRNA localization trends also provide another intriguing clue about the RNAi mechanisms. In the images with these siRNAs (Figs. 1 and 2), we observed that the NS3 and 7SK siRNAs localize selectively in the cytoplasm and nucleus, respectively, precisely the sites of the respective silencing target RNA molecules. Hence, these observations provide evidence for the existence of a mechanism by which the RNAi machinery influences the passive or active transport and localization of the siRNA and corresponding RISC formation to subcellular compartments containing target RNA. To understand how siRNA duplexes are distributed in cells when no complementary target mRNA exists in the cell, we carried out similar experiments using CHO cells, which lack the cytoplasmic silencing target for NS3 siRNA, but carry the small nuclear 7SK and U6 target RNAs. After transfection in these cells, the "target-less" NS3 siRNA is distributed throughout both the cytoplasm and the nucleus of these cells, exhibiting only a low tendency for strand separation (Fig. 3*d*), a behavior very different from that of the same siRNA in Huh-7 cells. This result demonstrates that, when cells do not contain silencing target RNA, selective cytoplasmic or nuclear localization of siRNA and RISC complexes is no longer sustained.

Consistent with its behavior in Huh-7 and HeLa cells, 7SK siRNA once again localizes to the nucleus of CHO cells (Fig. 4). Additionally, to understand whether the observed nuclear localization of nuclear-targeted siRNA is specific to 7SK, analogous experiments were also carried out with an siRNA targeting the small nuclear U6 RNA (6, 17) in HeLa cells. A similar selective nuclear localization was also observed in this case (Fig. 8, which is published as supporting information on the PNAS web site), as well as in Huh-7 and CHO cells (data not shown), showing that this effect is a more general feature of nuclear-targeted siRNAs. Taken together, the imaging results with the three siRNA duplexes in multiple cell lines support a mechanism where the target RNA location determines the localization and function of siRNA and RISC.

Imaging experiments carried out 24 h after transfection provided additional information on later stages of the RNAi process. Huh-7 and CHO cells transfected with NS3 siRNA do not display significant changes in siRNA distributions at 24 h after transfection, still showing either clear strand separation and only clustered antisense strand throughout the cytoplasm (Huh-7 cells), or the accumulation of largely intact duplexes throughout the cytoplasm and the nucleus (CHO cells). On the other hand, Huh-7 and CHO cells transfected with 7SK siRNA, and examined 24 h after transfection, revealed an

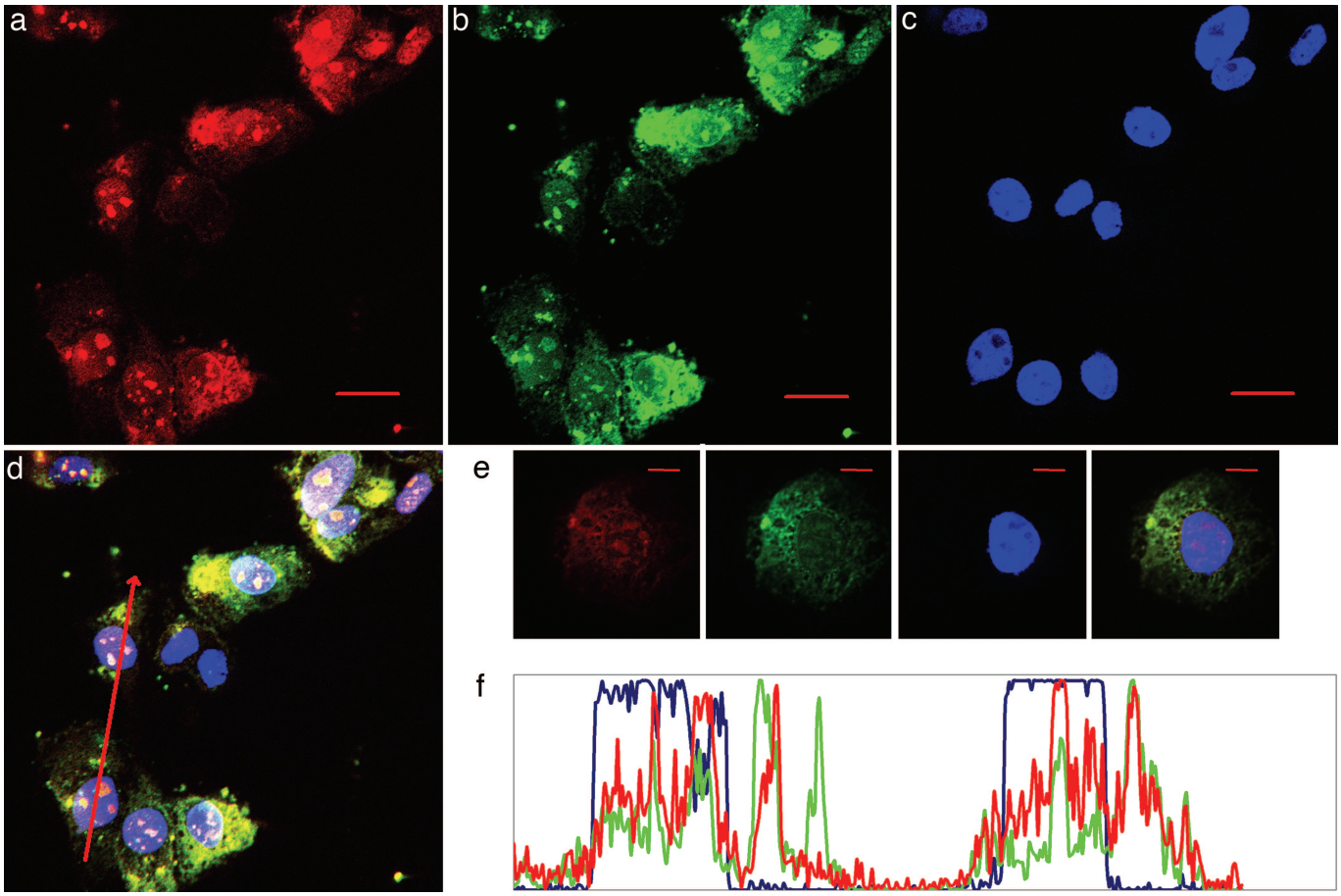

Fig. 3. NS3 siRNA distributes into the cytoplasm as well as the nucleus in CHO cells 2 h after transfection. (*a–c*) NS3 siRNA antisense (red) and sense (green) strands are seen throughout the cytoplasm and the nucleus (blue). (Scale bar, 20 μm.) (*d*) Overlay of red, green, and blue. (e) A single cell. (Scale bar, 10 μm.) (*f*) Intensity profiles along the selected line (red arrow in *d*) across two cells.

altered pattern of siRNA distribution. The antisense strand remains somewhat localized to the nucleus, being trapped mostly in the nucleoli (Fig. 5), but also shows significant spreading into the cytoplasm. Most remarkably, the sense strand was only observed at very low levels in the cytoplasm of a few cells, showing its absence not only in the nucleus but also nearly completely from the entire cell (Fig. 5*d*). Although not a direct observation of RISC movement, these observations may signify that nuclear-formed active RISCs are translocated into the cytoplasm at later stages of the nuclear RNAi pathway, as a consequence of or during the completion of the nuclear RNA decay pathway. Additional studies will be needed to further clarify this aspect of the nuclear RNAi mechanism.

Although the specific molecular basis for a target RNA biased siRNA localization is yet to be understood, our observations are consistent with a mechanism where the siRNA/RISC are trapped at cellular sites or in compartments containing the target RNA, via a specific targeting machinery or repeated cycles of target-binding, cleavage, and release. Along these lines, after incorporation of the antisense strand of NS3 siRNA into active RISC in the cytoplasm, it could be targeted as a RISC constituent to cytoplasmic centers of RNA decay, thus "trapping" the antisense strand of cytoplasmic targeted siRNA in the cytoplasm. Processing (P) or cytoplasmic bodies have recently been described as such centers for final degradation of mRNA by decapping enzymes and exonucleases (20, 21), and the studies have demonstrated the colocalization of RISC associated Ago1 and Ago2 proteins with these cytoplasmic centers, proposing a link between P-bodies and RNAi pathway in the cytoplasm (7–9, 22). On the other hand, our results show that the absence of a cytoplasmic target RNA results in a lack of 7SK and U6 siRNA target-associated trapping in the cytoplasm. Instead, these siRNAs effectively translocate to the nucleus, where a core cleavage protein (Ago2) is also located, as shown (6–9), and confirmed in our imaging experiments of Ago2 intracellular distribution by expressing Myc-tagged Ago2 in HeLa cells and visualizing it by using anti-Myc Alexa Fluor 555-conjugated antibody (data not shown). Nuclear active siRNAs likely form active RISCs directly in the nucleus, and therefore may be "trapped" at sites containing nuclear 7SK and U6 target RNAs. Additionally, the extent of this nuclear trapping appears reduced 24 h after transfection, and the antisense siRNA strand redistributes into the cytoplasm, whereas the sense strand, presumably cleaved by the Ago2 protein at the onset of RISC assembly (10, 11), fully decays. In line with the above scenario, the lack of a target RNA at any location in CHO cells eliminates all such trap sites for NS3 siRNA, and this siRNA is distributed throughout these cells.

In conclusion, our findings provide insights into the functioning of the RNAi machinery in mammalian cells. We find that cytoplasmically active RISC formation is likely not a common step in the cytoplasmic and nuclear RNAi pathways. Rather, for nuclear RNAi, active RISC appears to be formed in the nucleus. Our results also provide evidence for a mechanism by which the RNAi machinery influences the transport and localization of the

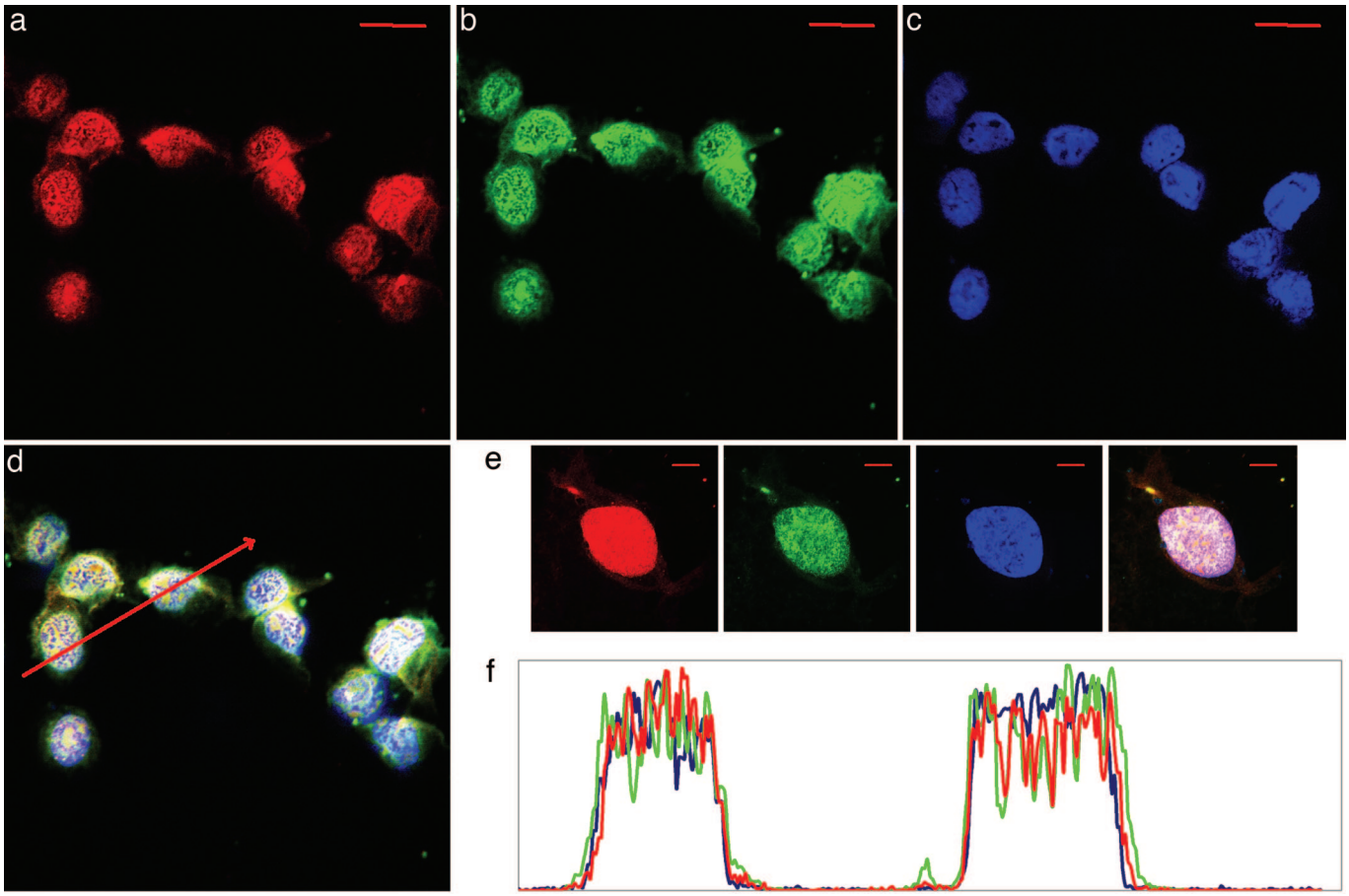

Fig. 4. 7SK siRNA localizes primarily to the nucleus in CHO cells 2 h after transfection. (*a–c*) 7SK siRNA antisense (red) and sense (green) strands accumulate in the nucleus (blue), showing very low cytoplasmic distribution. (Scale bar, 20 μm.) (*d*) Overlay of red, green, and blue. (*e*) A single cell. (Scale bar, 10 μm.) (*f*) Intensity profiles along the selected line.

corresponding siRNA and RISC to target RNA sites. Such a mechanism could serve a functional role in RNAi pathways by colocalizing the active RISC and its target RNA. Our studies reinforce the idea of RNAi as a phenomenon with multiple cellular pathways. They also provide evidence that subcellular compartmentalization may have a significant impact on RISC assembly and function, while raising the question of what specific molecular mechanisms are responsible for the observed selective localization.

Materials and Methods

RNAi Assay. The 7SK siRNA (sense strand 5′-CCUCCAAACAAGCUCUCAAdTdT-3′) targets nucleotides 220–238 of the 7SK small nuclear RNA, and the U6 siRNA (sense strand 5′-AAUUGGAACGAUACAGAGAdTdT-3′) targets nucleotide 29–48 of the U6 RNA (6). The HCV replicon NS3 siRNA (sense strand 5′-CCCAAAUGUACACCAAUGUdTdT-3′) targets the NS3 portion of the viral genome. All siRNAs were purchased from Dharmacon as single strands, and duplexes were annealed in different pairwise combinations of fluorescently labeled (Alexa Fluor 488 at the 3′ end of the sense strand, Cy5 at the 3′ end of the antisense strand) and unlabeled strands. 7SK small nuclear RNA knockdown was evaluated by using quantitative PCR, measured in cells mock-transfected (control) or transfected with unlabeled, antisense (Cy5) labeled, and antisense (Cy5) plus sense (Alexa Fluor 488) labeled 7SK siRNAs. One microgram of total RNA from transfected CHO cells was reverse transcribed. 7SK levels were normalized to 18S ribosomal RNA and are presented relative to RNA levels in mock-transfected cells (representative of three independent experiments, Fig. 6). Down-regulation of HCV replicon level by NS3 siRNAs was evaluated by transfection of Huh-7 cells harboring pFK-I389 neo/luc with the NS3 siRNA unlabeled and with antisense Cy5, sense Alexa Fluor 488, and Cy5 plus Alexa Fluor 488 labeled. Their effects on the replicon level (luciferase assay) were measured after 48 h. All values were normalized relative to mock transfection (Fig. 7).

Cell Culture, DNA Construct, and Transfection. The human hepatoma Huh-7 cell line harboring subgenomic HCV replicon was generated as described (23). Huh-7, CHO, and HeLa cell lines were cultured in RPMI medium 1640 (CHO, HeLa) and DMEM (10% FBS), respectively, at 37°C with 5% CO_2. For imaging, cells were cultured overnight in two-well glass-coverslip bottom chambers (Lab-Tek) at 50% confluence and transfected with 200 pmol of fluorescently labeled siRNAs by Lipofectamine 2000 (Invitrogen) in OptiMEM. At the end of transfection, the cells were washed three times with PBS and stained with DAPI used at 1:1,000 for 1 min (Sigma). Myc-tagged Ago2 plasmids as described in ref. 8 were provided by Roy Parker (University of Arizona, Tucson). Cells were transfected with DNA plasmids by Mirus (Madison, WI) TransIT-LT1. Transfected cells were fixed by using 3% paraformaldehyde (in PBS) for 12 min at room temperature and permeabilized by using 0.2% Triton X-100 in PBS for 6 min at 4°C. Anti-Myc Tag, clone 4A6, Alexa Fluor 555 conjugate

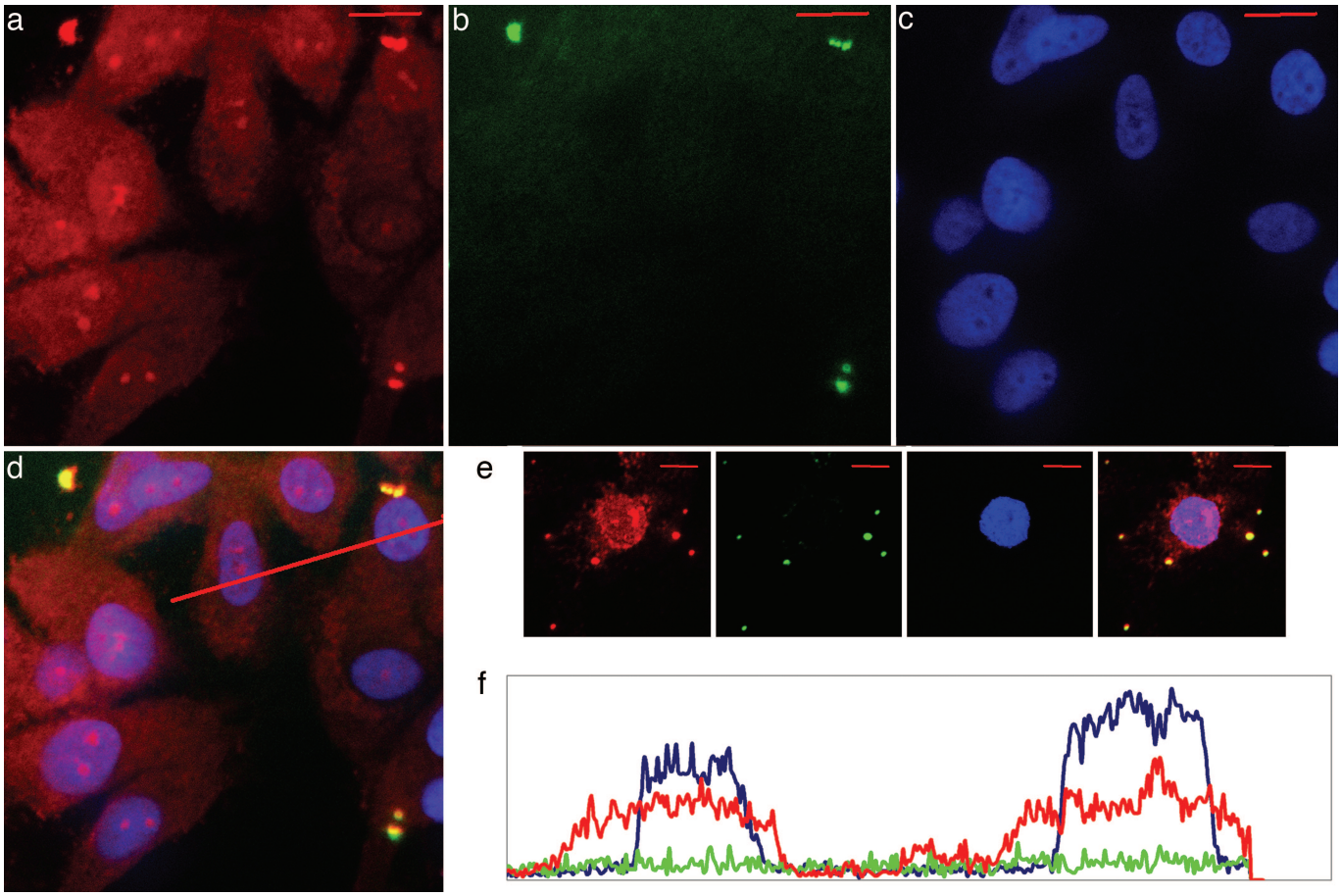

Fig. 5. 7SK siRNA distributes throughout CHO cells 24 h after transfection. (*a–c*) 7SK siRNA antisense strand (red) is seen in the cytoplasm and the nucleus, whereas sense strand (green) gets eliminated. (*d*) Colocalization shows antisense strand is retained in the nucleoli (red spots) and confirms integrity of the cell nuclei (blue). (Scale bar, 20 μm.) (e) A single cell. (Scale bar, 10 μm.) (*f*) Intensity profiles along the selected line.

(mouse monoclonal IgG1) (Upstate Biotechnology, Lake Placid, NY) was applied according to manufacturer's protocol.

Confocal Imaging. Bio-Rad–Zeiss Radiance 2100 LSM with a ×60, 1.4 numerical aperture oil immersion objective was used for data acquisition and analysis (The Scripps Research Institute Microscopy Core Facility). Fluorophores were excited by using blue diode at 406 nm, argon–ion at 488 nm, 543 nm HeNe green, and 647 nm red diode lasers. For transfected cells showing siRNA inside, we plotted signal profiles for all three dyes along various selected lines, crossing through the cell (Zeiss LSM IMAGE EXAMINER 3.5 software). In total, 110–130 transfected cells were quantitatively analyzed in four separate experiments for each of the described combinations of siRNA type and cell line.

We thank G. B. Robb and T. M. Rana (University of Massachusetts, Amherst) for providing information on the 7SK and U6 siRNA sequences, R. Parker (University of Arizona, Tucson) for Myc-tagged Ago2 plasmids, R. Bartenschlager (University of Heidelberg, Heidelberg) for HCV replicon plasmid, members of the A.A.D. laboratory for discussions, and Emily Remba for help with the figures. This work was supported by The Scripps Research Institute, National Institutes of Health Grant GM 073104 (to A.A.D.), and Department of Energy Grant ER46051 (to P.G.S.).

1. Fire, A., Xu, S., Montgomery, M. K., Kostas, S. A., Driver, S. E. & Mello, C. C. (1998) *Nature* **391,** 806–811.
2. Morris, K. V., Chan, S. W., Jacobsen, S. E. & Looney, D. J. (2004) *Science* **305,** 1289–1292.
3. Kawasaki, H. & Taira, K. (2004) *Nature* **431,** 211–217.
4. Langlois, M. A., Boniface, C., Wang, G., Alluin, J., Salvaterra, P. M., Puymirat, J., Rossi, J. J. & Lee, N. S. (2005) *J. Biol. Chem.* **280,** 16949–16954.
5. Haussecker, D. & Proudfoot, N. J. (2005) *Mol. Cell. Biol.* **25,** 9724–9733.
6. Robb, G. B., Brown, K. M., Khurana, J. & Rana, T. M. (2005) *Nat. Struct. Mol. Biol.* **12,** 133–137.
7. Sen, G. L. & Blau, H. M. (2005) *Nat. Cell Biol.* **7,** 633–636.
8. Liu, J., Valencia-Sanchez, M. A., Hannon, G. J. & Parker, R. (2005) *Nat. Cell Biol.* **7,** 719–723.
9. Liu, J., Rivas, F. V., Wohlschlegel, J., Yates, J. R., III, Parker, R. & Hannon, G. J. (2005) *Nat. Cell Biol.* **7,** 1261–1266.
10. Matranga, C., Tomari, Y., Shin, C., Bartel, D. P. & Zamore, P. D. (2005) *Cell* **123,** 607–620.
11. Rand, T. A., Peterson, S., Du, F. & Wang, X. (2005) *Cell* **123,** 621–629.
12. Meister, G. & Tuschl, T. (2004) *Nature* **431,** 343–349.
13. Sontheimer, E. J. (2005) *Nat. Rev. Mol. Cell Biol.* **6,** 127–138.
14. Hügle, T., Fehrmann, F., Bieck, E., Kohara, M., Kräusslich, H. G., Rice, C. M., Blum, H. E. & Moradpour, D. (2001) *Virology* **284,** 70–81.
15. Gurney, T., Jr., & Eliceiri, G. L. (1980) *J. Cell Biol.* **87,** 398–403.
16. Wassarman, D. A. & Steitz, J. A. (1991) *Mol. Cell. Biol.* **11,** 3432–3445.
17. Matera, A. G. & Ward, D. C. (1993) *J. Cell Biol.* **121,** 715–727.
18. Randall, G., Grakoui, A. & Rice, C. M. (2003) *Proc. Natl. Acad. Sci. USA* **100,** 235–240.
19. Martinez, J. & Tuschl, T. (2004) *Genes Dev.* **18,** 975–980.
20. Cougot, N., Babajko, S. & Seraphin, B. J. (2004) *Cell Biol.* **165,** 31–40.
21. Sheth, U. & Parker, R. (2003) *Science* **300,** 805–808.
22. Rossi, J. (2005) *Nat. Cell Biol.* **7,** 643–644.
23. Vrolijk, J. M., Kaul, A., Hansen, B. E., Lohmann, V., Haagmans, B. L., Schalm, S. W. & Bartenschlager, R. C. (2003) *J. Virol. Methods* **110,** 201–209.